Quantum Dynamics in Condensed Phase: Charge Transfer in Biological Systems and Organic Photovoltaics

by

NSHUTI Jean Paul
April 2024

Supervisor: Prof. Fabien GATTI
Co-supervisor: Dr. Steve NDENGUE

This master's thesis is submitted to East African Institute for Fundemental Research for partial fulfillment of the requirement of Master's Degree

Abstract

The simulation of nonadiabatic dynamics in the condensed-phase system provides a better understanding of photoinduced electron transfer within biological systems. The Caretenoid(C) Porpyrin(P) Fullerene(C_{60}) explicitly dissolved in Tetrahydrofuran is used as a prototypical organic photovoltaics triad molecule due to its properties of mimicking photosynthetic process. The simulations employ the Multi-state Harmonic model (MSH) Hamiltonian developed in ref [1] which provides the strategy of describing real Hamiltonian for systems of multiple electronic states. In this work, we simulate the nonadiabatic photoinduced electron transfer dynamics using a full quantum dynamics approach of MCTDH (Multi-configuration Time-Dependent Hartree) and its extension of ML-MCTDH and compare it with semiclassical models. The three-state case was found out that can reproduce semiclassical results but the four-state case failed to reproduce the semiclassical results.

Acknowldgement

I would like to express my sincere gratitude to each and everyone who contributed to the successful completion of this work. Your prayers, guidance, encouragement and support have been vital throughout this journey.

First, I want to thank my supervisors Professor Fabien GATTI and Dr. Steve Ndengue for their great guidance, expertise and mentorship. Their work was important to accomplish this work.
I am also grateful to Mr. Lei SHI for his guidance, knowledge sharing and assistance he provided during this work. His work and advice were encouragement for me.

I extend my gratitude to the International Center of Theoretical Physics (ICTP) through the East African Institute for Fundemental Research (EAIFR) for giving me the opportunity and guidance to pursue my master's courses, I also thank the World Academy of Science (TWAS) for providing the scholarship grant.
Moreover, I want to thank the *Institut des Sciences Moléculaires d'Orsay*(ISMO) for giving me the greatest opportunity for a six-month internship and providing me with the required computational resources.

I would like to acknowledge the support from family, friends and colleagues who were on my side during this time. Your prayers, help, and encouragement were necessary for this work.
Lastly, I appreciate all the participants and collaborators for their generous contribution and their time, Without them this project would not have been possible.

Sincerely,

NSHUTI Jean Paul

Contents

Abstract **ii**

Acknowldgement **iii**

1 Introduction **2**

2 Theory **5**
2.1 Quantum dynamics 5
2.2 Molecular Model 6
2.3 Multi-state Harmonic Model Hamiltonian 9

3 Methodology **11**
3.1 MCTDH 11
3.1.1 Wavefunction Ansatz and Equation of motion 11
3.2 Multi-Layer MCTDH 13
3.3 Electronic States 14
3.4 Relaxation in MCTDH 15
3.5 Thermalization in MCTDH 16

4 Numerical Simulation **18**
4.1 Thermalization 18
4.2 Photoexcitation 19
4.3 Propagation of wavepackets 19

5 Results and Discussion **22**
5.1 Convergences Test 22
5.2 60-Modes system 23
5.3 Population transfer 24
5.3.1 Three-state case 24
5.3.2 Four-state case 25

6 Conclusion **27**

A Population dynamics of Semi-Classical approach for the three-state case **28**

B Population dynamics of Semi-Classical approach for the four-state case **28**

References **33**

List of Figures

1 Photoinduced electron transfer process 3
2 CPC_{60} molecular triad 7
3 ML-tree structure 14
4 The Multi-layer tree representation for 60 mode system 21
5 Convergence in primitive basis after thermalization 22
6 Population transfer dynamics between the excited state {$\pi\pi^*$,CT1,CT2} 23
7 Population dynamics after Thermalization 24
8 Population dynamics between two excited states { $\pi\pi^*$, CT1 } in the three-state case 25
9 Population dynamics between the excited states {$\pi\pi^*$, CT1 and CT2 } in the four-state case 26
10 Population dynamics of CT2 26
11 Population dynamics of the different semi-classical methods for the three-state case 28
12 Population dynamics of different semi-classical methods for the four-state case. 29

List of Tables

1 The electronic coupling between pairs of electronic states 19

1 Introduction

In our everyday life, we always need energy and most of the energy sources nowadays are based on fossil fuels like coal, oil, and natural gas which have driven society for a very long time and now they are depleting. The world demand for energy is rising and the environment must be conserved, which is why the world needs to find a versatile and clean source of energy. Solar energy is one of the promising solutions for the world energy crisis due to its versatility, green, and mostly being renewable source [2].

In recent years, Organic Photovoltaics (OPV) devices have attracted the attention of researchers and have been potentially considered due to their low costs of production, green, and flexibility. The efficiency of OPVs is lower compared to inorganic photovoltaics because of their band gap [3]. The conversion of energy in OPV devices is built based on two fundamental processes; Photoinduced charge transfer (CT) where the organic layers absorb the sunlight and generate the electron-hole pair bounded together by electrostatic force; The spectrum of sunlight and the energy gap of the organic material should be related closely [4, 5] and excitation energy transfer (EET) [6].

The main challenges for Organic photovoltaics (OPVs) are the low Power Conversion Efficiency (PCE) and short lifetime. One of the key factors that influence the PCE is The absorption efficiency which is determined by how the energy gap is related to the solar spectrum. Most OPV materials have large band gaps which does not allow them to capture the maximum amount of photon, the best way of overcoming this, is to narrow the band gap of donor molecules. Narrowing the bandgap allow the absorption of more photon. Another big challenge for OPVs is absorption irreversibility, the organic materials used in OPVs degrade due to exposure to sunlight or other form of light. To improve the efficiency of OPVs we need to study the link between quantum coherence and the chemical structure of OPVs molecules. Understanding the quantum dynamics between donor and acceptor molecules gives insight into the population transfer within the molecular triad.

A Carotenoid Porphyrin Fullerene (CPC_{60}) molecule explicitly dissolved in a solvent of Tetrahydrofuran (THF) is an excellent example of an artificial photosynthetic material that mimics the process of natural photosynthesis.[7]
In the process of simulating the Photoinduced CT, The system (CPC_{60} dissolved in THF) is equilibrated on its ground state (G) state at 300K, in this state CPC_{60} triad and THF solvent are in thermal equilibrium. After that vertical photoexcitation occurs to P-localized excited state $\pi\pi^*$, CP^*C_{60}, Then it is followed by nonradiative transition to excited P-to-C_{60} CT state, $CP^+C_{60}^-$ which is called CT1, or to the excited C-to-C_{60} charge separation state, $C^+PC_{60}^-$ known as CT2. The development of an effective Hamiltonian with multiple electronic states for a condensed phase system was developed in [1] and specifically this model was studied in [8].

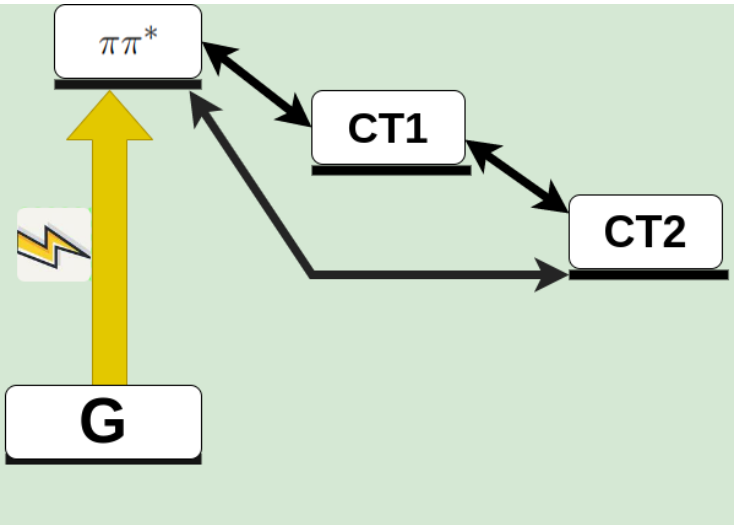

Figure 1: Photoinduced electron transfer process

The accurate simulation of nonadiabatic dynamics based on molecular models is one of the key roles in learning about the concept of charge and energy transfer in condensed phase systems [9, 10], which may result in the discovery of solar energy conversion materials with more efficiency [11]. One of the widely used theories of estimating CT rate constant in condensed-phase systems is Marcus theory [12, 13, 14, 15]. In the Marcus theory approach, only three parameters are used in the expression of CT rate constants: the reaction free energy (ΔE), the electronic coupling coefficient between donor and acceptor, and the reorganization energy. What's more, Marcus theory provides the best way to understand CT rates, not only that, it also helps to interpret the CT rates obtained Experimentally [16]. Marcus theory may not be very good for the simulating transfer of charges within a condensed phase system, it is preferable to develop new approaches for calculating CT rates. However, the simulation in the condensed-phase system may be complicated due to the fluctuations of surrounding "solvents" molecules, intermolecular interactions, and electron-vibration coupling[17].

However, many semi-classical approaches are employed for understanding the nonadiabatic dynamics in Condensed phase systems like Linearized Semiclassical (LSC) [18], Symmetrical Quasiclassical (SQC) methods [19], spin mapping model [20], mixed quantum-classical Liouville (MQCL) [21] and classical mapping model. All these methods are combined in what is called a mixed-quantum classical scheme which uses quantum wavefunction to describe electrons whereas classical mechanics is used to treat nuclear motion. While the Mean-field approach is the propagation of classical trajectory over the average potential of

electronic states [22]. All these methods share the same challenge of combining classical and quantum theories [23].

The nonadiabatic dynamics can also be studied using quantum dynamics approaches like full quantum wavepacket dynamics, Multiconfiguration Time-Dependent Hartee (MCTDH)[24], its extension of Multi-layer MCTDH (ML-MCTDH) for a very large system [25], and Gaussian-based MCTDH (G-MCTDH) [26].

In this work, we aim to simulate the photoinduced electron transfer in the nonadiabatic dynamics system. To do the quantum dynamics simulation with full dimensionality is very difficult, that is why we employed ML-MCTDH which is very good for simulating time-dependent quantum dynamics of systems with very large degrees of freedom (DOF). We will also check the validity of the semiclassical method. This dynamical approach will allow us to study the population transfer between different electronic excited states and compare our findings with the work in ref[8], where they simulate the electron transfer dynamics in a condensed phase by using the method of Meyer-Miller mapping Hamiltonian by empowering semiclassical and mixed-quantum classical dynamics methods like the linearized semi-classical, symmetrical quasiclassical, mean-field Ehrenfest, classical mapping model, and spin mapping model. Importantly, we wish to know the significance of the quantum effect on the electronic transfer dynamics at room temperature.

The rest of this thesis is structured as follows. The quantum dynamics theory, the molecule used, and the construction of Hamiltonian are summarized briefly in section 2. section 3 discuss about the theory of MCTDH. The simulation techniques and simulation details are provided in section 4. The results are discussed in section 5.

2 Theory

2.1 Quantum dynamics

In quantum mechanics, the description of the system is represented by the Hamiltonian operator $\hat{H}$. The solution of Schrödinger's equation gives the behavior of the quantum system.

$$\hat{H}\left|\psi_n\right\rangle = E_n\left|\psi_n\right\rangle \tag{2.1}$$

The equation 2.1 is known as Time Independent Schrödinger's Equation (TISE), where ψ represent the eigenstate of the system and E_n is the eigenvalues energies of the system. The combinations of the set of eigenstates $\{|\psi_n\rangle\}$ can be used to describe the quantum wavefunction. Solving the schrödinger equation exactly leads to the determination of all physical quantities of the system.
To describe the dynamics of a system that evolves over time like the reaction rate, population transfer, and others, we have to solve the Time Dependent Schrödinger's equation (TDSE).

$$\hat{H}\psi(r,t) = \imath\hbar\frac{\partial\psi(r,t)}{\partial t} \tag{2.2}$$

The solution of Equation 2.2 is;

$$\psi(r,t) = e^{-\imath\hat{H}t/\hbar}\psi(r,t=0) \tag{2.3}$$

Where the evolution operator is given by $e^{-\imath\hat{H}t/\hbar}$. This solution is associated with two cases;

1. At a reference time (assume $t = 0$) one of the eigenfunctions of Equation 2.1 is equal to the wavefunction;

   $$\psi(r,t=0) = \psi_n(r) \tag{2.4}$$

   Substitute Equation 2.4 into Equation 2.3, which gives;

   $$\psi(r,t) = e^{-\imath E_n t/\hbar}\psi_n(r) \tag{2.5}$$

   This state has a periodic time dependence with the angular frequency $\omega = E_n/\hbar$. The measurable quantity can give the information about the system, let's take an example of the probability density.

   $$\begin{aligned} |\psi(r,t)|^2 &= \psi^*(r,t)\psi(r,t) \\ &= \psi_n^*(r)e^{\imath E_n t/\hbar}e^{-\imath E_n t/\hbar}\psi_n(r) \\ &= \psi_n^*(r)\psi_n(r) \end{aligned} \tag{2.6}$$

   So, the probability density is time-independent which means the system does not evolve over time and has definite energy E_n for each state.

2. At $t = 0$, and the wavefunction is expressed as a linear combination of the eigenstates given by Equation 2.1

$$\psi(r, t = 0) = \sum_n C_n \psi_n(r) \tag{2.7}$$

Where C_n is the expansion coefficient and can be used to determine the overlap between wavefunction and eigenfunction;

$$C_n = \int \psi_n^*(r)\psi(r, t = 0)dr \tag{2.8}$$

The probability of measuring the energy of the system E_n is equal to $|C_n|^2$.

At time ($t \neq 0$), the wavefunction can be determined by substituting Equation 2.7 into Equation 2.3 which then give;

$$\begin{aligned} \psi(r, t) &= e^{-\imath \hat{H} t/\hbar} \sum_n C_n \psi_n(r) \\ &= \sum_n C_n e^{-\imath \hat{H} t/\hbar} \psi_n(r) \\ &= \sum_n C_n e^{-\imath E_n t/\hbar} \psi_n(r) \end{aligned} \tag{2.9}$$

This equation gives the time-dependent state in the discrete case which is also known as *wavepackets*. The exact solution of TDSE for all time gives the dynamical and physical properties of the system. However, the exact solution of TDSE is very hard to get due to different reasons like the complexity of the quantum system, dimensionality of wavefunction, interactions and potentials, and boundary conditions. Hence, the exact solution is possible for only simple systems.

There are many approximations that have been used for studying the complex system like, the Born-Oppenheimer approximation which is about separating the nuclear and electronic motion. It relies on the theory that; the nuclear is much heavier than the electron which implies that the electrons move very fast and consider nuclear as stationary [27]. There are many methods that are based on this approximation like DFT, which provides the approximate solution of the TISDE for electrons at fixed nuclear coordinates, which is used then to provide the potential energy surface (PES) of electrons.

2.2 Molecular Model

The molecular architecture of natural plants helps them to convert solar energy into chemical energy efficiently. The way natural plants mastered the light-harvesting process is fascinating and can provide a better understanding of how photoexcitation should be achieved by combining light-absorbing molecules [28].

The main challenge is how to design a molecular model that can convert solar energy efficiently as natural plants do so, that it can be used in electric power generation.

A good example of such a prototypical molecular model is covalently linked Carotenoid (C), Porphyrin (P), and Fullerene (C_{60}) solvated in explicit Tetrahydrofuran (THF) solvent [29, 30]. This molecule is a potential candidate for the simulation of electron transfer dynamics because it mimics certain processes of photoinduced electron transfer as photosynthetic material. The molecular model is composed of Carotene which has a protective role, It is also composed of a light-absorbing Porphyrin ring which works as an electron donor, and photoreaction center fullerene which acts as an electron acceptor [31].

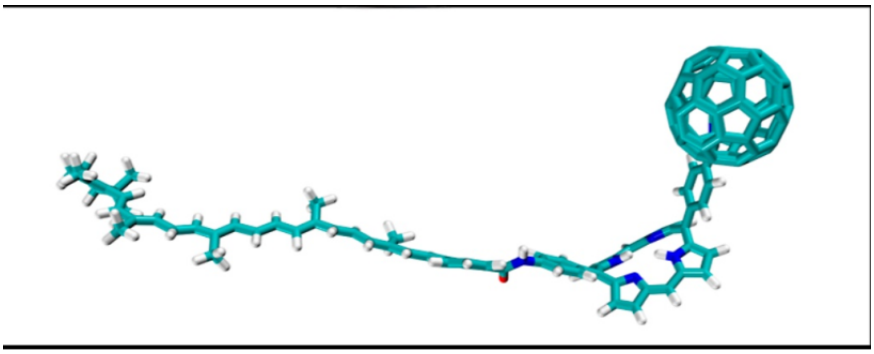

Figure 2: CPC_{60} molecular triad in explicit THF solvent, THF is not shown for clear visualization [8]

This molecular model possesses some properties and interactions that suit well the process of electron transfer, some of those properties are as follows:

- Comparable energy levels: the efficiency of electron transfer depends on the distinct energy levels within the molecular model; the way energy levels are aligned in CPC_{60} enables its effective electron transfer. Carotenoids usually have a HOMO-LUMO energy gap in the same range as visible light wavelengths, allowing them to absorb the solar spectrum in that range. After absorbing the photon it gets excited to a higher-energy state, and the electron, which was in HOMO, gets excited to LUMO which makes it available for further transfer [32].

  The HOMO energy level of porphyrin is matched with the LUMO of carotenoids which allows the photoexcited electron to transfer from carotenoids to porphyrin. And the electron at porphyrin HOMO can be easily transferred to the electron acceptor (fullerene). In general, fullerenes are better electron acceptor because their LUMO energy levels are lower than porphyrins' HOMO energy levels. The transfer of photoexcited electrons from

porphyrins to fullerene is dominant because of energy alignment between them which makes it easy for electrons to fall to fullerene LUMO which results in the creation of a charge-separated state [33].

- Tunable properties, The CPC_{60} properties can be easily controlled and optimized for achieving efficient electron transfer. Tuning of energy levels plays a big role in controlling the energy landscape of the system like, The rising or lowering of energy levels affects the alignment of donor-acceptor energy levels which changes the charge separation.

- Tetrahydrofuran as a solvent, To achieve very efficient photoinduced electron transfer depends on the polarity of the surrounding environment (solvent). Tetrahydrofuran has a moderate polarity with a dielectric constant of 7.6, which allows the dissolution of both polar and nonpolar compounds. For efficient electron transfer, a solvent with a moderate dielectric constant is suitable because it does not affect a lot the electrostatic interactions and ensures the homogeneity of the solution.

2.3 Multi-state Harmonic Model Hamiltonian

In many applications of molecular dynamics, the nuclear degree of freedom (DOF) is treated as a bath, while electronic DOF is treated as a system. So to be able to perform the simulation, we have to construct the system-bath Hamiltonian.
The MSH model Hamiltonian is given by:

$$\hat{H} = \begin{bmatrix} \hat{H}_1 & \hat{\Gamma}_{12} & \hat{\Gamma}_{13} & \dots & \hat{\Gamma}_{1F} \\ \hat{\Gamma}_{21} & \hat{H}_2 & \hat{\Gamma}_{23} & \dots & \hat{\Gamma}_{2F} \\ \hat{\Gamma}_{31} & \hat{\Gamma}_{32} & \hat{H}_3 & \dots & \hat{\Gamma}_{3F} \\ \vdots & \vdots & \vdots & \ddots & \vdots \\ \hat{\Gamma}_{F1} & \hat{\Gamma}_{F2} & \hat{\Gamma}_{F3} & \dots & \hat{H}_F \end{bmatrix} \tag{2.10}$$

For the system of N nuclear modes and F electronic states. The nuclear Hamiltonian is given by the $(F-1) \times N$ dimensional extended configuration space.

The four-state MSH Hamiltonian model is given by:

$$\begin{cases} \hat{H}_1 = \sum_{\alpha=1}^{F-1} \sum_{j=1}^{N} \frac{\hat{P}_{\alpha,j}}{2} + \sum_{j=1}^{N} \frac{1}{2}\omega_j^2 [\hat{R}_{1,j}^2 + \hat{R}_{2,j}^2 + ... + \hat{R}_{F-1,j}^2] + \varepsilon_1 \\ \hat{H}_2 = \sum_{\alpha=1}^{F-1} \sum_{j=1}^{N} \frac{\hat{P}_{\alpha,j}}{2} + \sum_{j=1}^{N} \frac{1}{2}\omega_j^2 [(\hat{R}_{1,j} - S_j^{(12)})^2 + \hat{R}_{2,j}^2 + ... + \hat{R}_{F-1,j}^2] + \varepsilon_2 \\ \hat{H}_3 = \sum_{\alpha=1}^{F-1} \sum_{j=1}^{N} \frac{\hat{P}_{\alpha,j}}{2} + \sum_{j=1}^{N} \frac{1}{2}\omega_j^2 [(\hat{R}_{1,j} - S_j^{(13)})^2 + (\hat{R}_{2,j} - S_j^{(23)})^2 + ... + \hat{R}_{F-1,j}^2] + \varepsilon_3 \\ ... \\ \hat{H}_F = \sum_{\alpha=1}^{F-1} \sum_{j=1}^{N} \frac{\hat{P}_{\alpha,j}}{2} + \sum_{j=1}^{N} \frac{1}{2}\omega_j^2 [(\hat{R}_{1,j} - S_j^{(1F)})^2 + (\hat{R}_{2,j} - S_j^{(2F)})^2 + ... + (\hat{R}_{F-1,j} - S_j^{(F-1,F)})^2] + \varepsilon_F \end{cases} \tag{2.11}$$

Where ω_j is the frequency of j-th normal mode (j=1, 2, ...,N), the electronic couplings $\hat{\Gamma}_{XY}(X \neq Y)$ is the same ($\hat{\Gamma}_{XY} = \hat{\Gamma}_{YX} = \Gamma_{XY}$) in condon aproximation. $\varepsilon_\alpha(\alpha = 1, \dots, F)$ is the adiabatic minimum energy of the $\alpha-$state, and then $S_j^{(XY)}(x \neq Y)$ is the equilibrium shift components for the PES of state α-state [8, 1, 11].

It is possible to get ε_α from electronic structure calculations, through the optimized geometries of all electronic states or use MD simulation to compute the reaction-free energy [1].
To obtain the equilibrium shift $S_j^{(XY)}$, one needs first to obtain the time correlation coefficients (TCFs) of the energy gap from the MD simulation. The

TCFs energy gap between two PESs can be defined as;

$$C_{UU}^{(XY)}(t) = \langle U_{XY}(t)U_{XY}(0)\rangle - \langle U_{XY}\rangle^2 \tag{2.12}$$

Where U_{XY} is the energy gap and it is equal to the difference between the PESs of the distinct state. From TCF we can be able to calculate the reorganization-free energy $E_r^{(XY)}$.

$$E_r^{(XY)} = \frac{C_{UU}^{(XY)}}{2K_BT} \tag{2.13}$$

Then the equilibrium shifts $S_j^{(XY)}$ between each pair of states are proportional to the square root of the reorganization energy.

$$S_j \sim \sqrt{E_r^{(XY)}} \tag{2.14}$$

To determine the constant of proportionality, we need to project the PESs shift vectors $\{V_{ij}\}$ to the distinct axis by considering the angle between each state. The formulation of this Hamiltonian involves a lot of work and was developed in the group of Dr. X. Sun (New York University Shanghai).

3 Methodology

3.1 MCTDH

In this chapter, we will present the Multiconfiguration Time-Dependent Hartree Method (MCTDH) method. The MCTDH was introduced in the 90s by Meyer, Manthe, and Cederbaum[24]. This approximation method was designed for solving a time-dependent Schrödinger equation.

3.1.1 Wavefunction Ansatz and Equation of motion

In the MCTDH theory the wavefunction *Ansatz* is used to solve time-dependent schrödinger's equation and it is written as: [34, 35]

$$\Psi(q_1, ..., q_f, t) = \sum_{j_1}^{n_1} ..... \sum_{j_f}^{n_f} A_{j_1 \dots j_f}(t) \prod_{\kappa=1}^{f} \varphi_{j_\kappa}^{(\kappa)}(q_\kappa, t) \tag{3.1}$$

The set of basis functions φ^κ are called single-particle functions (SPF_S). The time-independent basis sets are used to express the SPFs:

$$\varphi_{j_\kappa}^{(\kappa)}(q_\kappa, t) = \sum_{i_\kappa}^{N_\kappa} c_{i_\kappa}^{(\kappa, j_\kappa)}(t) \chi_{i_\kappa}^{(\kappa)}(q_\kappa) \tag{3.2}$$

where $\chi_{i_\kappa}^{(\kappa)}(q_\kappa)$ is a primitive basis function, which is a DVR (Discrete Variable Representation) function that depends on coordinate q_k. To derive the MCTDH equation of motion we need to rewrite (3.1) as :

$$\Psi(q_1, ..., q_f, t) = \sum_J A_J \Phi_J \tag{3.3}$$

$$= \sum_{j=1}^{(\kappa)} \varphi_j^{(\kappa)} \Psi_j^{(\kappa)} \tag{3.4}$$

Where we introduced composite indices notation:

$$J \equiv (j_1, \dots, j_f)$$
$$A_J \equiv A_{j_1 \dots j_f}$$
$$\Phi_J \equiv \Pi_{\kappa=1}^{f} \varphi_{j_\kappa}^{(\kappa)}$$

Dirac-Frenkel variational principal [36] is used to approximate the solution of the time-dependent Schrödinger equation. This guarantees that the chosen wavefunction is as close as possible to the exact solution of TDSE.

$$\langle \delta\Psi | H - \imath \frac{\partial}{\partial t} | \Psi \rangle \tag{3.5}$$

Where $\delta\Psi$ is the variational of wavefunction. The variation with respect to coefficient and SPFs yield a configuration and single-hole functions, respectively,

$$\frac{\delta\Psi}{\delta A_J} = \Phi_J \tag{3.6}$$

$$\frac{\delta\Psi}{\delta\varphi_j^{(\kappa)}} = \Psi_j^{(\kappa)} \tag{3.7}$$

The derivative of the wavefunction with respect to time is given by:

$$\dot{\Psi} = \sum_J \dot{A}_J \Phi_J + \sum_{j=1}^{f}\sum_{j=1}^{n_\kappa} \dot{\varphi_J}^{(\kappa)} \Psi_j^{(\kappa)} \tag{3.8}$$

By substituting (3.4) in (3.5). And consider the variational with respect to the coefficients. For δA_J:

$$\imath\dot{A}_J = \sum_L \langle\Phi_J|H|\Phi_L\rangle\, A_L - \imath\sum_{k=1}^{f}\sum_{l=1}^{n_\kappa} g_{j_k l}^{(\kappa)} A_{J_l^\kappa} \tag{3.9}$$

Where

$$g_{j_\kappa l}^{(\kappa)} = \langle\varphi_j^{(\kappa)}|g^{(\kappa)}|\varphi_l^{(\kappa)}\rangle = \imath\,\langle\varphi_j^{(\kappa)}|\dot{\varphi}_l^{(\kappa)}\rangle \tag{3.10}$$

Next, consider the variations with respect to the SPF_S. For $\delta\varphi_j^\kappa$

$$\imath\dot{\varphi}_j^{(\kappa)} = \sum_{k,l} (\rho^{(\kappa)-1})_{jk}(1-P^{(\kappa)})\,\langle H\rangle_{kl}^\kappa\,\varphi_l^{(\kappa)} \tag{3.11}$$

Where we introduced the projection operator,

$$P^{(\kappa)} = \sum_{j=1}^{n_\kappa} |\varphi_j^{(\kappa)}\rangle\,\langle\varphi_j^{(\kappa)}| \tag{3.12}$$

And for $g^{(\kappa)} \equiv 0$. We can get the following equation of motion:

$$\begin{aligned} \imath\dot{A}_J &= \sum_L \langle\Phi_J|H|\Phi_L\rangle\, A_L \\ \imath\dot{\varphi}_j^{(\kappa)} &= \sum_{k,l} (\rho^{(\kappa)-1})_{jk}(1-P^{(\kappa)})\,\langle H\rangle_{kl}^\kappa\,\varphi_l^{(\kappa)} \end{aligned} \tag{3.13}$$

Introduce The SPFs vector

$$\varphi^{(\kappa)} = (\varphi_1^{(\kappa)} \dots \varphi_{n_\kappa}^{(\kappa)})^T \tag{3.14}$$

Last equation of 3.13 can be rewritten as;

$$\imath\dot{\varphi}^{(\kappa)} = (1-P^{(\kappa)})\rho^{(\kappa)^{-1}}\,\langle H\rangle^{(\kappa)}\,\varphi^{(\kappa)} \tag{3.15}$$

Hence, the full general equation of motion of MCTDH becomes;

$$\begin{aligned} \imath\dot{A}_J &= \sum_L \langle\Phi_J|H|\Phi_L\rangle\, A_L - \sum_{\kappa=1}^{f}\sum_{l=1}^{n_\kappa} g^{(\kappa)}_{j_\kappa l} A_{J^\kappa_l} \\ \imath\dot{\varphi}^{(\kappa)} &= (1-P^{(\kappa)})[\rho^{(\kappa)^{-1}}\langle H\rangle^{(\kappa)} - g^{(\kappa)}\mathbf{1}]\varphi^{(\kappa)} + (g^{(\kappa)}\mathbf{1})\varphi^{(\kappa)} \end{aligned} \tag{3.16}$$

This equation of motion is derived using the Variational Principle, to ensure that the mean energy and the norm of the wavepacket are conserved during propagation. This EOM are coupled differential equations which can be solved using Runge-Kutta or Adams-Bashforth-Moulton integrators.

The main problem for the other quantum dynamics methods like the standard method is that the primitive basis size increases as the dimension (number of degrees of freedom) of the system increases. To minimize this problem MCTDH uses single-particle functions (SPFs) which are time-dependent (Equation 3.2), which evolve with the system during propagation. Furthermore, the number of SPF functions used is smaller than the number of basis functions for primitive basis sets, which will give flexibility in the numerical effort related to computation time. However, the problem of dimensionality is not solved completely and other techniques like mode combination and ML-MCTDH are employed to tackle the problem.

3.2 Multi-Layer MCTDH

This is the extension of MCTDH which is suitable for solving the more complex Quantum Dynamics problem i.e. the problem with higher dimensionality. In this way, the Degree of freedom (DOF) that can be accommodated by the SPF group increased. In trying to solve this, we have to re-express *Ansatz* as many times as possible by creating a series of layers that are connected by time-dependent basis functions.[25, 35, 34]. To avoid clumsy notation let us consider a four-dimensional case.

An ML-MCTDH wavefunction with 3 layers will look like:

$$\Psi(q_1,q_2,q_3,q_4,t) = \sum_{j_{12}=1}^{n_{12}}\sum_{j_3}^{n_{34}} A_{j_{12},j_{34}}(t)\varphi^{(12)}_{j_{12}}(q_1,q_2,t)\varphi^{(34)}_{j_3}(q_3,q_4,t) \tag{3.17}$$

Where

$$\begin{aligned} \varphi^{(12)}_{j_{12}}(q_1,q_2,t) &= \sum_{k_1=1}^{n_1}\sum_{k_2=1}^{n_2} B^{(12,j_{12})}_{k_1,k_2}(t)\xi^{(1)}_{k_1}(q_1,t)\xi^{(2)}_{k_2}(q_2,t) \\ \varphi^{(34)}_{j_{34}}(q_3,q_4,t) &= \sum_{k_3=1}^{n_1}\sum_{k_4=1}^{n_4} B^{(34,j_34)}_{k_3,k_4}\xi^{(3)}_{k_3}(q_3,t)\xi^{(4)}_{k_3}(q_4,t) \end{aligned} \tag{3.18}$$

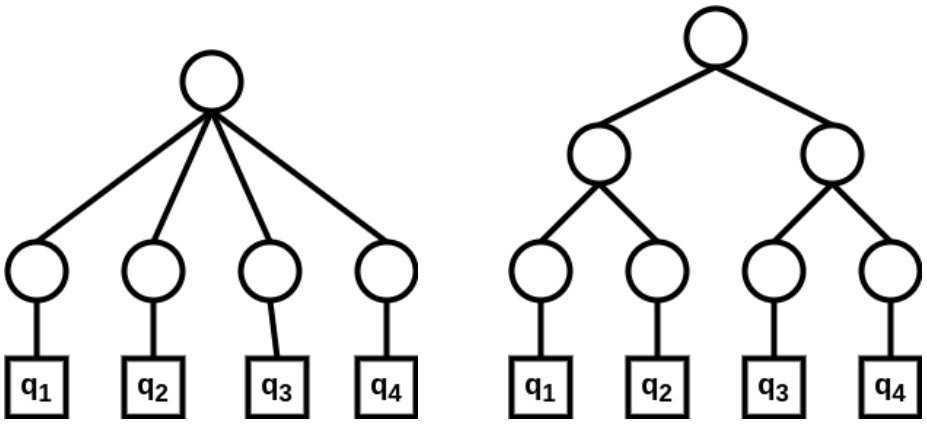

(a) (b)

Figure 3: Example of the tree structure of MCTDH and ML-MCTDH wavefunction. (a) The wavefunction is expanded into a SPFs basis which then expanded into a primitive basis. (b)The wavefunction is expanded into two SPFs (two-dimensional second layer) which are also expanded into third layer(one-dimensional) SPFs which then expanded into a primitive basis.

And,

$$\begin{aligned}
\xi^{(1)}_{k_1}(q_1,t) &= \sum_{i_1=1}^{N_1} C^{(1,k_1)}_{i_1}(t)\chi^{(1)}_{i_1}(q_1) \\
\xi^{(2)}_{k_2}(q_2,t) &= \sum_{i_2=1}^{N_2} C^{(2,k_2)}_{i_2}(t)\chi^{(2)}_{i_2}(q_2) \\
\xi^{(3)}_{k_3}(q_3,t) &= \sum_{i_3=1}^{N_3} C^{(3,k_3)}_{i_3}(t)\chi^{(3)}_{i_3}(q_3) \\
\xi^{(4)}_{k_4}(q_4,t) &= \sum_{i_2=1}^{N_4} C^{(4,k_4)}_{i_4}(t)\chi^{(4)}_{i_4}(q_4)
\end{aligned} \tag{3.19}$$

In Equation 3.18, the SPF functions are expressed in terms of new SPF instead of time-independent basis set functions which form another layer. For a very large system, ML-MCTDH is more efficient than MCTDH and it is capable of treating systems with hundreds of nuclear degrees of freedom.

3.3 Electronic States

The MCTDH methods can be applied to systems with multiple electronic states. To handle this system we have to add the extra degree of freedom which represents the electronic manifold [37]. In this formalism, the wavefunction can be

written as follows:

$$|\Psi\rangle = \sum_{j_1}^{n_1} ... \sum_{j_f}^{n_f} \sum_{\alpha=1}^{n_s} A_{j_1 ... j_f^\alpha} \varphi_{j_1}^{(1)}(q_1, t) ... \varphi_{j_f}^{f}(q_f, t) \, |\alpha\rangle \tag{3.20}$$

This formalism is known as *Single-set* because all electronic states share the same set of SPFs. On the other hand, there is so-called *multi-set* formalism where each state uses a different set of SPFs.

$$|\Psi\rangle = \sum_{\alpha=1}^{n_s} \psi_\alpha(q_1, ..., q_f, t) \, |\alpha\rangle \tag{3.21}$$

Here the component of ψ_α can be written in MCTDH form as follows:

$$\psi_\alpha(q_1, ..., q_f, t) = \sum_{j_1^\alpha}^{n_1^\alpha} ... \sum_{j_f^\alpha}^{n_f^\alpha} A^{(\alpha)}_{j_1^\alpha ... j_f^\alpha}(t) \varphi_{j_1}^{(1,\alpha)}(q_1, t) ... \varphi_{j_f^\alpha}^{(f,\alpha)}(q_f, t) \tag{3.22}$$

The EOM has to be generalized

$$\begin{aligned} \imath \dot{A}_J^{(\alpha)} &= \sum_{\beta=1}^{n_1^\alpha} \sum_L \mathcal{K}_{JL}^{(\alpha,\beta)} A_L^{(\beta)} \\ \imath \dot{\varphi}_j^{\kappa,\alpha)} &= (1 - P^{(\kappa,\alpha)})(\rho^{(\kappa)})_{jl}^{(-1)} \sum_{\beta=1}^{n_s} \sum_{k=1}^{n_\kappa^\alpha} \mathcal{H}_{lk}^{(\kappa,\alpha,\beta)} \varphi_k^{(\kappa,\beta)} \end{aligned} \tag{3.23}$$

Where,

$$\begin{aligned} \mathcal{K}_{JL}^{(\alpha,\beta)} &= \langle \Phi_J^{(\alpha)} | H^{(\alpha,\beta)} | \Phi_L^{(\beta)} \rangle \\ \mathcal{H}_{jl}^{(\kappa,\alpha,\beta)} &= \langle \Psi_j^{(\kappa,\alpha)} | H^{(\alpha,\beta)} | \Psi_l^{(\kappa,\beta)} \rangle \end{aligned} \tag{3.24}$$

The multi-set formalism is more efficient and preferable in many cases.

3.4 Relaxation in MCTDH

all derivation in this section are taken from ref [38]

The relaxation method is the process of obtaining the ground state wavefunction by a time-dependent method (propagation in negative imaginary time). Which then turns the schrödinger equation into:

$$\dot{\Psi} = -H\Psi \tag{3.25}$$

To solve the effect, one has to expand the WF as a function eigenstate of Hamiltonian.

$$\psi(t) = \sum_n a_n e^{-E_n t} \Psi_n \tag{3.26}$$

Let us denote "E_0" as the lowest energy state, which will win. And of course, the norm must be conserved. To conserve the norm of Ψ, we have to introduce the Lagrange multiplier in the schrödinger's equation.

$$\dot{\Psi}(t) = -(H - E(t))\Psi(t) \quad \text{where } E(t) = \langle\Psi(t)|H|\Psi(t)\rangle \tag{3.27}$$

Then,

$$\langle\Psi(t)|\dot{\Psi}(t)\rangle = 0 \quad \Rightarrow \frac{d}{dt}\|\Psi\|^2 \tag{3.28}$$

Where E is the Lagrange multiplier and assumes Ψ to be normalized. By differentiating $E(t)$ with respect to t, we get:

$$\dot{E}(t) = -\langle\Psi(t)|(H - E(t))^2|\Psi(t)\rangle \tag{3.29}$$

As time increases the WF will converge towards the ground state due to a decaying exponential function. In relaxation, as the relaxation time increases, energy decreases and converges if the WF becomes the eigenstate of Hamiltonian[35, 37]. The relaxation will work well when there is an overlap between the ground state and initial state Ψ.

3.5 Thermalization in MCTDH

The thermalization of the wavefunction is a process of equilibrating the system's temperature. In MCTDH, it involves propagating the wave packets in imaginary time (relaxation), where a statistical sampling scheme is used to obtain the propagated initial wave packets.
Here is the calculation of the partition function by employing the statistical sampling:

$$Q(T) = tr(e^{-\hat{H}\beta}) = \sum_n \langle\varphi_n|e^{-\hat{H}\beta}|\varphi_n\rangle \tag{3.30}$$

where φ_n is the set of orthonormal basis functions which has to satisfy completeness relation. The explicit sum over all basis function is forbidden due to numerical effort, the alternative way of skipping the summation is to use a statistical sampling scheme. Let's introduce the statistical wavefunction ψ_j which has to satisfy also the completeness relation.

$$|\psi_j\rangle = \sum_n (-1)^{\alpha_n(j)} |\varphi_n\rangle \tag{3.31}$$

And the completeness relation;

$$\lim_{M\to\infty} \frac{1}{M} \sum_{j=1}^{M} |\psi_j\rangle \langle\psi_j| = 1 \tag{3.32}$$

where $\alpha_n(j)$ is the integer random number.
Use equation (3.31) to compute the trace of $e^{-\hat{H}\beta}$.

$$\begin{aligned} tr(e^{-\hat{H}\beta}) &= tr\left(e^{-\hat{H}\beta} \lim_{M\to\infty} \frac{1}{M} \sum_{j=1}^{M} |\psi_j\rangle \langle\psi_j|\right) \\ Q(T) &= \lim_{M\to\infty} \frac{1}{M} \sum_{j=1}^{M} \langle\psi_j| e^{-\hat{H}\beta} |\psi_j\rangle \end{aligned} \tag{3.33}$$

Here M denotes the number of samples, and the statistical error increases as $1/\sqrt{M}$ as M increases. To get the exact values of the trace from a single statistical wavefunction ψ_j, the basis function φ_n has to be the eigenstate of the Hamiltonian $\hat{H}$.
To compute the partition function one needs to propagate M statistical wavefunction in imaginary time [39].

4 Numerical Simulation

The simulation details of CPC_{60} dissolved in THF are provided within this section. The model is composed of four electronic states which are: the ground state CPC_{60}; initial state $\pi\pi^*$ state, CP^*C_{60} state; the excited state, $CP^+C_{60}^-$ which indicated as CT1; and the excited $C^+PC_{60}^-$ indicated as CT2.
The photoinduced CT process takes place in two different cases:

1. The three-state case composed by { $\pi\pi^*$, CT1, G },
2. The four-state case composed by { $\pi\pi^*$, CT1, CT2, G }.

In this study, we will focus only on the three-state case. The simulation was performed in three main processes;

4.1 Thermalization

The system (all DOF) is equilibrated at the ground state (state 4) with T= 300k. The thermalization process is guided by Boltzmann distribution. In fact, Boltzmann distribution helps to determine the number of quantum states that are needed for a system to be in thermal equilibrium.

$$\langle n \rangle = \frac{1}{Z} \sum_n \frac{1}{e^{-\beta E_n}} \tag{4.1}$$

where $Z = \frac{2}{\sinh(\beta E_n)}$ is a partition function and $E_n = \omega/2$ is the energy of harmonic oscillator.

- Primitive basis is used to construct the single particle functions of an MCTDH [40]. The primitive basis representation we used is HO (Harmonic oscillator) and FFT (Fast Fourier transform). HO is used for modes with small grid sizes (usually below 100) while FFT is used for modes with large grid sizes so that it can speed up the calculation.
- For the MCTDH calculation initial wavefunction $\Psi(0)$ is essential and it is a linear combination of products of SPFs. The choice of initial wavefunction was based on the primitive basis, modes defined as HO in primitive basis have the initial wavefunction of Harmonic oscillator (HO) while the plane wave is used to define modes with FFT primitive basis.
- The construction of the ML-basis is based on combining several modes for reducing configuration space and computation time. The Figure 4 shows the ML tree of the system.

The computation of thermalization involves propagation in imaginary time up to the final time of $1/2KT$ with an integrator of 10^{-6}.

4.2 Photoexcitation

The process of photoexcitation involves the vertical electronic transition from the ground state referred to as (G) to the excited state referred to as the initial state ($\pi\pi^*$) within the Condon approximation [41]. To perform such a transition, we included the specific part in the Hamiltonian which takes the wavefunction from the electronic ground state (state 4) to the excited state (state 1). In this case, there is no electronic coupling between the ground state and the excited state.

4.3 Propagation of wavepackets

The simulation of nonadiabatic dynamics was performed in the three-state case. Where the three-state case involves electronic transfer from $\pi\pi^*$ to CT1, in this case, we only consider the electronic coupling between $\pi\pi^*$ and CT1 (Table 1).

Table 1: **The electronic couplings Γ_{XY} between different pairs of state (in eV) and the energy minima ε_α (in eV)**

Coupling	**Value**	**Energy minima**	**Values**
Γ_{12}	-1.5×10^{-2}	$\varepsilon(\pi\pi^*)$	0
Γ_{13}	7.2×10^{-3}	$\varepsilon(CT1)$	-0.828
Γ_{23}	-2.9×10^{-2}	$\varepsilon(CT2)$	-0.640
Γ_{j4}	0		

[a] This table shows the electronic states α =1,2,3, and 4 represent to $\pi\pi*$,CT1,CT2, and (G) respectively.

The wavepacket was propagated until $t = 400$ fs. Despite the propagation, the convergence of ML-basis requires a very large number of SPFs.

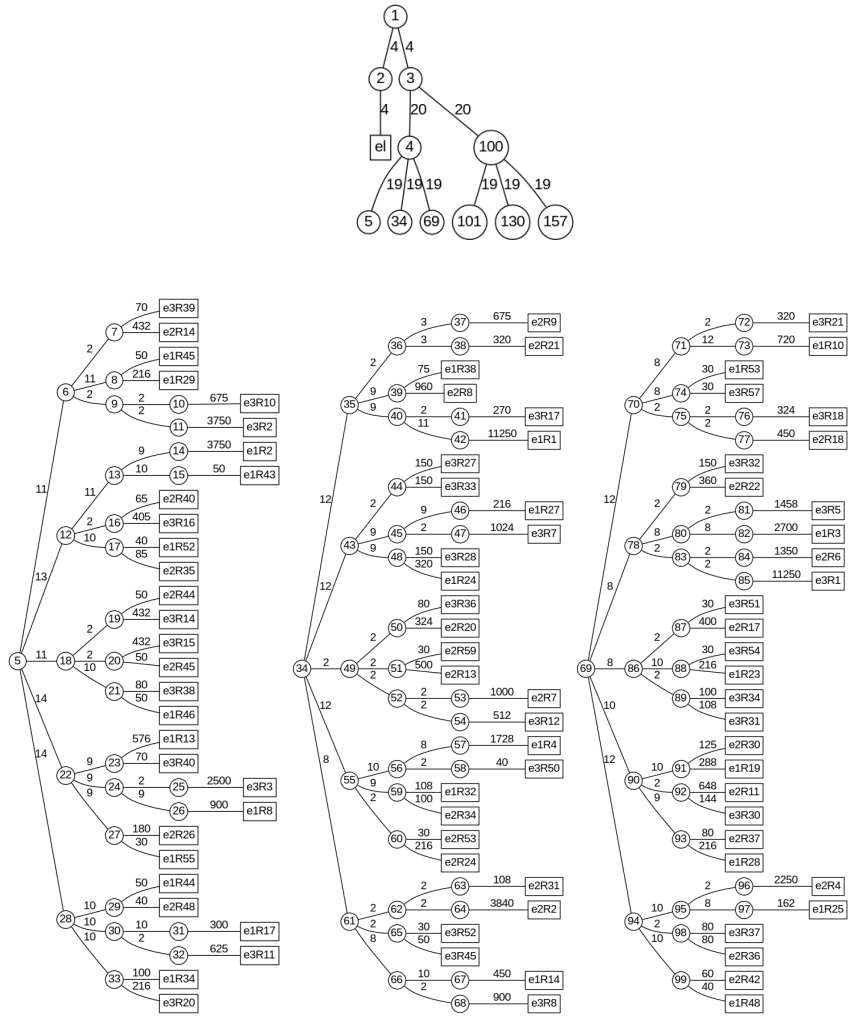
1
4
4
2
3
4
20
20
el
4
100
19
19
19
19
19
19
5
34
69
101
130
157
e3R39
70
7
432
e2R14
2
e1R45
50
8
216
e1R29
6
11
2
9
2
2
10
675
e3R10
11
3750
e3R2
9
14
3750
e1R2
13
10
15
50
e1R43
11
e2R40
65
16
405
e3R16
11
12
2
10
17
40
85
e1R52
e2R35
13
e2R44
50
19
432
e3R14
2
e3R15
432
20
50
e2R45
5
11
18
2
10
21
80
50
e3R38
e1R46
14
e1R13
576
23
70
e3R40
9
22
9
9
24
2
9
25
2500
e3R3
26
900
e1R8
14
27
180
30
e2R26
e1R55
e1R44
50
29
40
e2R48
10
28
10
10
30
10
2
31
300
e1R17
32
625
e3R11
33
100
216
e1R34
e3R20
(a)
3
37
675
e2R9
36
3
38
320
e2R21
2
75
e1R38
35
9
39
960
e2R8
9
40
2
41
270
e3R17
11
42
11250
e1R1
12
150
e3R27
44
150
e3R33
2
9
46
216
e1R27
43
9
45
2
47
1024
e3R7
9
48
150
320
e3R28
e1R24
12
80
e3R36
50
324
e2R20
2
34
2
49
30
e2R59
2
2
51
500
e2R13
12
52
2
53
1000
e2R7
2
54
512
e3R12
8
57
1728
e1R4
10
56
2
58
40
e3R50
55
9
59
108
e1R32
2
100
e2R34
60
30
e2R53
216
e2R24
2
63
108
e2R31
62
2
64
3840
e2R2
61
2
2
65
30
e3R52
8
50
e3R45
66
10
67
450
e1R14
2
68
900
e3R8
(b)
2
72
320
e3R21
71
12
73
720
e1R10
8
30
e1R53
74
8
30
e3R57
70
2
75
2
76
324
e3R18
2
77
450
e2R18
150
e3R32
79
360
e2R22
12
2
81
1458
e3R5
78
8
80
8
82
2700
e1R3
2
83
2
84
1350
e2R6
8
85
11250
e3R1
30
e3R51
87
400
e2R17
2
30
e3R54
69
8
86
10
88
216
e1R23
2
89
100
e3R34
10
108
e3R31
125
e2R30
91
288
e1R19
12
10
90
2
92
648
e2R11
9
144
e3R30
93
80
e2R37
216
e1R28
2
96
2250
e2R4
95
8
97
162
e1R25
10
94
2
98
80
e3R37
10
80
e2R36
99
60
e2R42
40
e1R48
(c)

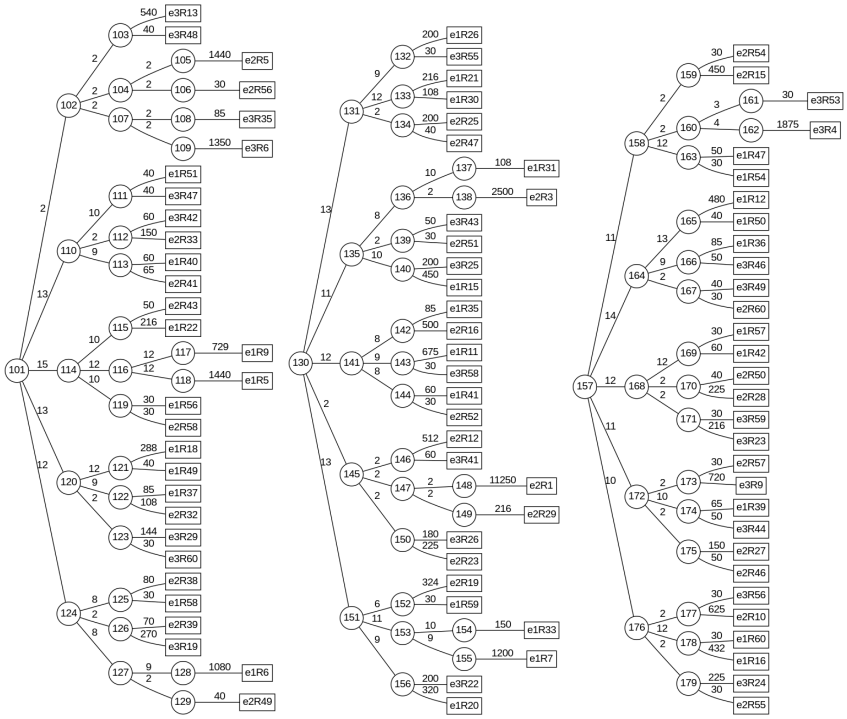

(d) (e) (f)

Figure 4: The Multi-layer tree representation for 60 mode system

5 Results and Discussion

5.1 Convergences Test

In the beginning, the system was comprised of 200 physical nuclear modes and four electronic states. This system has modes with very low frequencies, which makes it hard to converge. The system did not converge well in both momentum space and real space due to the large number of basis sizes used to represent the modes. The main challenge was to check convergence carefully for each mode in both real and momentum space. In MCTDH, momentum space is used to represent the kinetic part of the Hamiltonian while the real space is used for the spatial part of the Hamiltonian.
This system was thermalized at T = 300 k and gave the total energy of E_{tot} = 13.1336 eV which is low compared to 17.466 eV of theoretical energy.

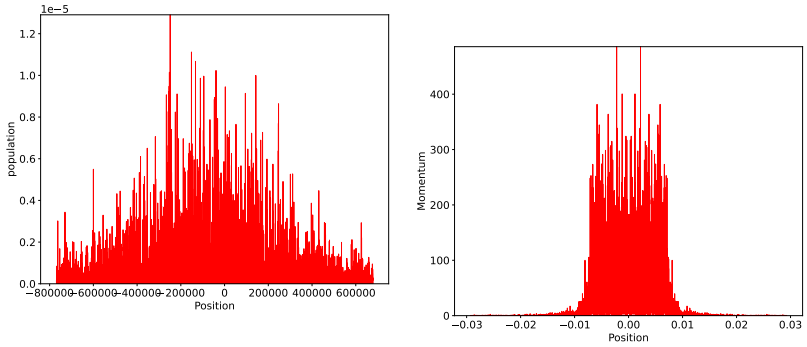

(a) (b)

Figure 5: Population dynamics of first degree of freedom (a) in real space and (b) momentum space.

The Figure 5 shows the population dynamics of the first degree of freedom in both real space and momentum space. This thermalization was not well converged, even if in momentum space looks well converged it is because we restrict the number of random states due to a lack of computational resources. Normally the numbers of random states should be equal to primitive basis size-1 and this mode has a very large basis size.

The purpose was to simulate the population dynamics between excited states, in (Figure 6) shows the population transfer from $\pi\pi^*$ to CT1 and CT2 in what we referred to as the four-state case. Due to couplings in Table 1 we expect to see large electron transfer from $\pi\pi^*$ to both CT1 and CT2. Instead, we observed the $\pi\pi^*$ population decay to 20% and only 0.00015% transferred to CT2. These results were very far from the semi-classical results presented in [8].
This system had a high computation time and its convergence in both primitive

and Multi-Layer bases was not converging well.

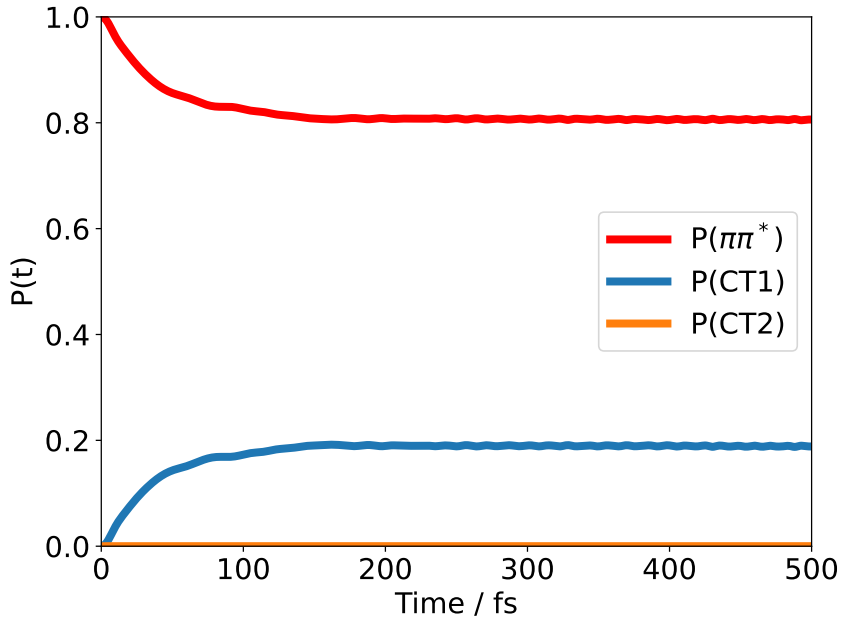

Figure 6: Population transfer dynamics between the excited state $\{\pi\pi^*$,CT1,CT2$\}$

5.2 60-Modes system

The new system is composed of 60 physical nuclear modes and 4 electronic states (G, $\pi\pi^*$, CT1, and CT2). The thermalization of the system gives the total energy $E_{tot} = 4.711$ eV at $T = 300K$ while the theoretical energy (zero-point energy + thermal energy) is $E = 5.29$ eV. The convergence was improved in both real and momentum space.

The Figure 7 shows two different degrees of freedom in both real and momentum representation. The previous calculation troubled to converge in primitive basis, this system converges well in both real and momentum space (Figure 7a) has better convergence than Figure 5). The modes that have been constructed within the HO basis clearly show that they follow Boltzmann distribution in momentum space (Figure 7d).

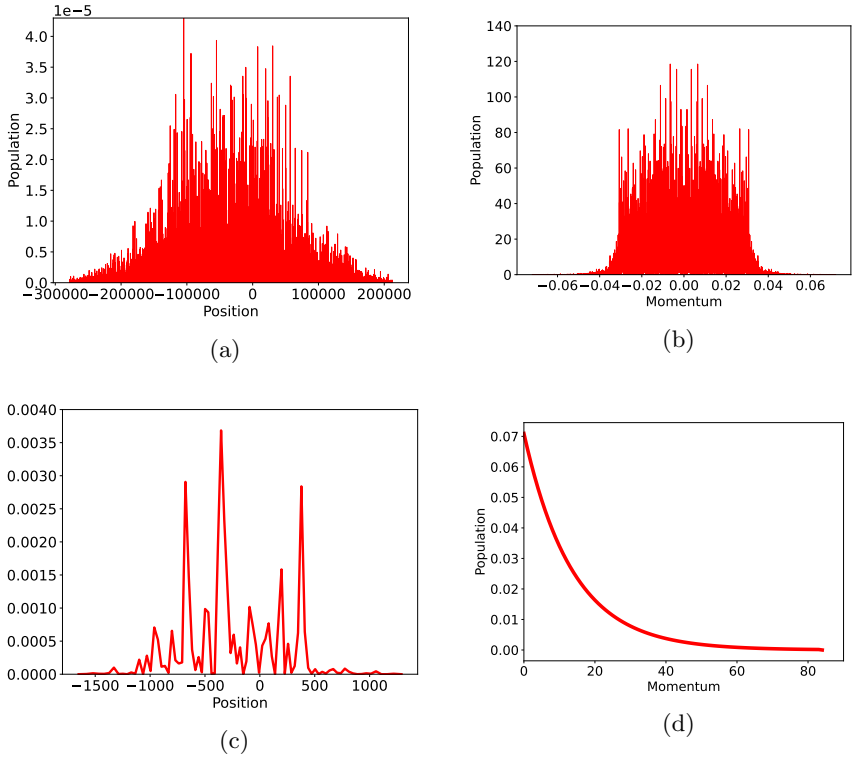

Figure 7: The population dynamics of (a) first degree of freedom in real space, (b) first degree of freedom in momentum representation, (c) 36^{th} DOF in real space, and 36^{th} DOF in momentum representation.

5.3 Population transfer

5.3.1 Three-state case

The obtained results from the nonadiabatic simulation of the three-state case are presented in Figure 8, The nonadiabatic dynamics show that after photoexcitation from the ground state to the initial state ($\pi\pi^*$), The population of ($\pi\pi^*$) decays to $70-75\%$ in the first 400 fs. In other words, due to the electronic coupling between $\pi\pi^*$ and CT1, there will be the electrons transfer from the initial state to the excited state (CT1). In the semi-classical approach, they found out that the population of the initial state ($\pi\pi^*$) decays to $60-80\%$ depending on the different dynamical methods they used (Figure A).
This clearly shows that quantum dynamics and semi-classical methods work well for a system of two excited states.

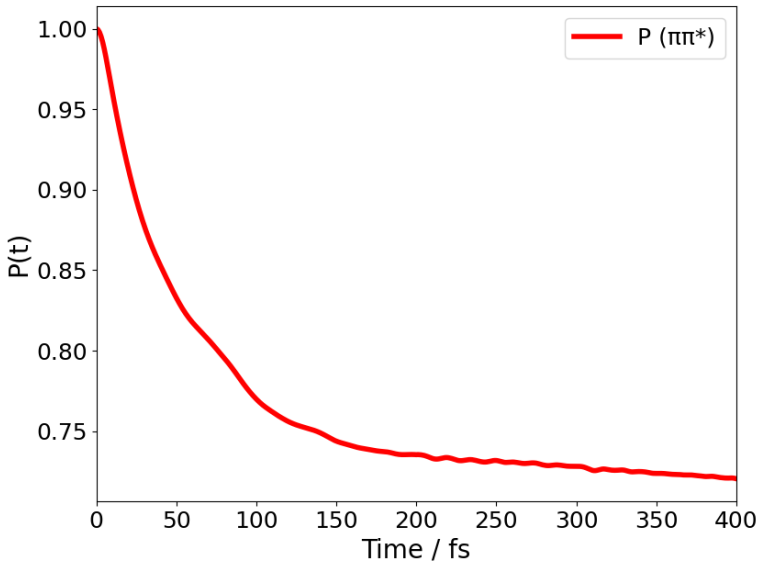

Figure 8: Population dynamics between two excited states { $\pi\pi^*$, CT1 } in the three-state case

5.3.2 Four-state case

The Figure 9 presents the nonadiabatic simulation results of the four-state case. In this case, after photoexcitation from ground state (G) to initial state ($\pi\pi^*$). The electronic transition between the excited states $\pi\pi^*$, CT1 and CT2 gives the population decay of the initial state to $60-70\%$ which is transferred to CT1 and CT2 but CT2 is not much populated as other states.
In the semi-classical approach, they found out that there is much population transfer to CT2 in the first 2 ps was up to $30-40\%$ and decays afterward (see Figure B).
The comparison between the quantum dynamics method and the semi-classical method shows that when three excited states are coupled, semi-classical methods fail. However, we can not conclude whether the semi-classical method fails or not, we still need to do many tests to be sure of it.

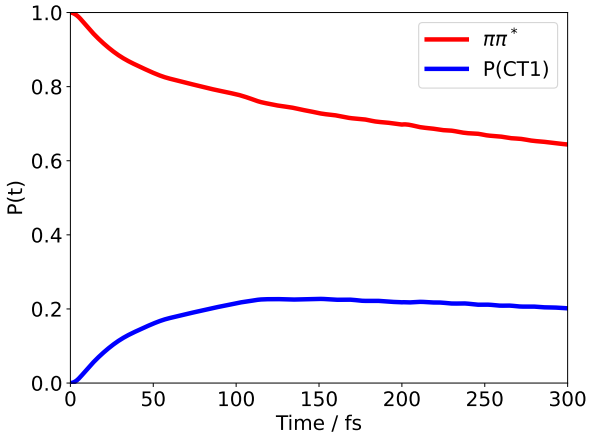

Figure 9: Population dynamics between the excited states $\{\pi\pi^*$, CT1 and CT2 $\}$ in the four-state case

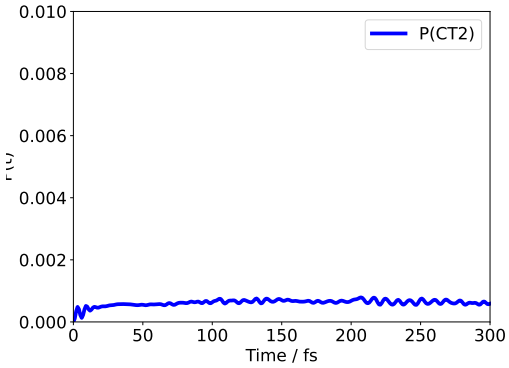

Figure 10: Population dynamics of CT2

I present the population dynamics of CT2 in Figure 10 for clear visualization. The CT2 electronic state is less populated than other states with a maximum population of 0.079%

6 Conclusion

In this work, we simulated the photoinduced electron transfer within a condensed-phase system made up of a Carotenoid-porphyrin-fullerene molecular triad dissolved in Tetrahydrofuran solvent using a full quantum dynamics approach. The Multi-configuration Time-dependent Hartree (MCTDH) method has been used to simulate the system.
The nuclear DOF was thermally equilibrated at the ground state and got vertical photoexcited to $\pi\pi^*$ initial electronic state which was followed by population transfer between excited states { $\pi\pi^*$, CT1} in the three-state case and { $\pi\pi^*$, CT1, CT2} in the four-state case. The non-adiabatic simulation in the three-state case reproduces the results within the same order as semi-classical results. However, the four-state fails to reproduce semi-classical results.
In the four-state case, due to the coupling between CT2 and other electronic states, we expected to see a large population transfer to CT2 instead we observed the difference. We are still investigating why the four-state case can not reproduce results in the same order as semi-classical results.

A Population dynamics of Semi-Classical approach for the three-state case

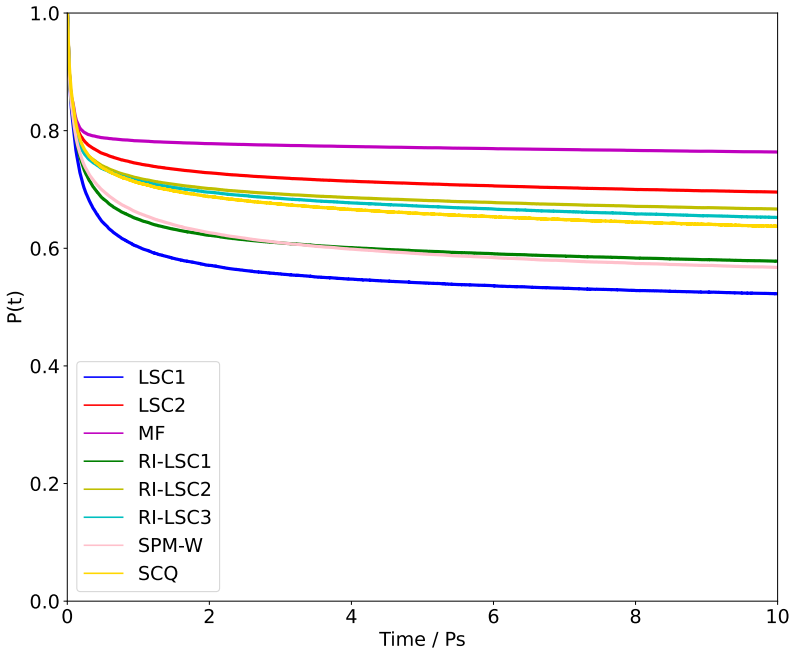

Figure 11: Population dynamics of the different semi-classical methods for the three-state case. This shows the population decay of $\pi\pi^*$ state

B Population dynamics of Semi-Classical approach for the four-state case

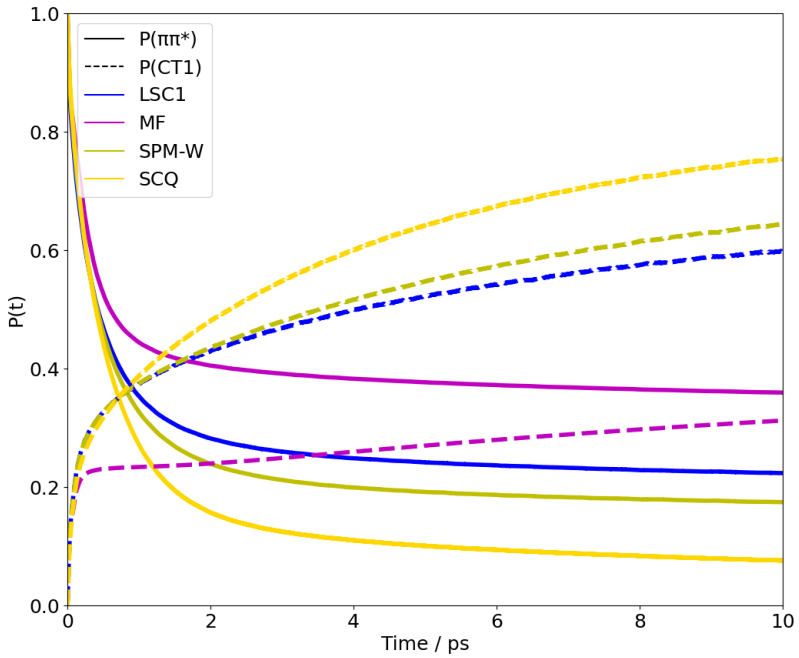

Figure 12: Population dynamics of different semi-classical methods for the four-state case.

References

[1] Z. Hu, D. Brian, and X. Sun, "Multi-state harmonic models with globally shared bath for nonadiabatic dynamics in the condensed phase," *The Journal of Chemical Physics*, vol. 155, no. 12, 2021.

[2] J. Xue, "Perspectives on organic photovoltaics," *Polymer Reviews*, vol. 50, no. 4, pp. 411–419, 2010.

[3] N. Yeh and P. Yeh, "Organic solar cells: Their developments and potentials," *Renewable and Sustainable Energy Reviews*, vol. 21, pp. 421–431, 2013.

[4] H. M. Heitzer, B. M. Savoie, T. J. Marks, and M. A. Ratner, "Organic photovoltaics: elucidating the ultra-fast exciton dissociation mechanism in disordered materials," *Angewandte Chemie*, vol. 126, no. 29, pp. 7586–7590, 2014.

[5] S. M. Falke, C. A. Rozzi, D. Brida, M. Maiuri, M. Amato, E. Sommer, A. De Sio, A. Rubio, G. Cerullo, E. Molinari, *et al.*, "Coherent ultrafast charge transfer in an organic photovoltaic blend," *Science*, vol. 344, no. 6187, pp. 1001–1005, 2014.

[6] J. Wang, Z. Zheng, Y. Zu, Y. Wang, X. Liu, S. Zhang, M. Zhang, and J. Hou, "A tandem organic photovoltaic cell with 19.6% efficiency enabled by light distribution control," *Advanced Materials*, vol. 33, no. 39, p. 2102787, 2021.

[7] Z. Tong, X. Gao, M. S. Cheung, B. D. Dunietz, E. Geva, and X. Sun, "Charge transfer rate constants for the carotenoid-porphyrin-c60 molecular triad dissolved in tetrahydrofuran: The spin-boson model vs the linearized semiclassical approximation," *The Journal of Chemical Physics*, vol. 153, no. 4, 2020.

[8] Z. Hu and X. Sun, "All-atom nonadiabatic semiclassical mapping dynamics for photoinduced charge transfer of organic photovoltaic molecules in explicit solvents," *Journal of Chemical Theory and Computation*, vol. 18, no. 10, pp. 5819–5836, 2022.

[9] K. Vandewal, "Interfacial charge transfer states in condensed phase systems.," *Annual review of physical chemistry*, vol. 67, pp. 113–33, 2016.

[10] A. Alavi, L. J. Álvarez, S. R. Elliott, and I. R. Mcdonald, "Charge-transfer molecular dynamics," *Philosophical Magazine Part B*, vol. 65, pp. 489–500, 1992.

[11] D. Brian, Z. Liu, B. D. Dunietz, E. Geva, and X. Sun, "Three-state harmonic models for photoinduced charge transfer," *The Journal of Chemical Physics*, vol. 154, no. 17, 2021.

[12] R. A. Marcus, "Electron transfer reactions in chemistry. theory and experiment," *Rev. Mod. Phys.*, vol. 65, pp. 599–610, Jul 1993.

[13] R. A. Marcus, "On the theory of oxidation-reduction reactions involving electron transfer. i," *The Journal of chemical physics*, vol. 24, no. 5, pp. 966–978, 1956.

[14] R. A. Marcus, "Electrostatic free energy and other properties of states having nonequilibrium polarization. i," *The Journal of Chemical Physics*, vol. 24, no. 5, pp. 979–989, 1956.

[15] R. A. Marcus, "Electron transfer reactions in chemistry: theory and experiment (nobel lecture)," *Angewandte Chemie International Edition in English*, vol. 32, no. 8, pp. 1111–1121, 1993.

[16] P. F. Barbara, T. J. Meyer, and M. A. Ratner, "Contemporary issues in electron transfer research," *The Journal of Physical Chemistry*, vol. 100, no. 31, pp. 13148–13168, 1996.

[17] Y. A. Berlin, F. C. Grozema, L. D. Siebbeles, and M. A. Ratner, "Charge transfer in donor-bridge-acceptor systems: Static disorder, dynamic fluctuations, and complex kinetics," *The Journal of Physical Chemistry C*, vol. 112, no. 29, pp. 10988–11000, 2008.

[18] M. A. Saller, A. Kelly, and J. O. Richardson, "On the identity of the identity operator in nonadiabatic linearized semiclassical dynamics," *The Journal of chemical physics*, vol. 150, no. 7, 2019.

[19] J. Zheng, Y. Xie, S.-s. Jiang, Y.-z. Long, X. Ning, and Z.-g. Lan, "Ultrafast electron transfer with symmetrical quasi-classical dynamics based on mapping hamiltonian and quantum dynamics based on ml-mctdh," *Chinese Journal of Chemical Physics*, vol. 30, no. 6, pp. 800–810, 2017.

[20] N. Prokof'Ev and P. Stamp, "Theory of the spin bath," *Reports on Progress in Physics*, vol. 63, no. 4, p. 669, 2000.

[21] N. Rekik, C.-Y. Hsieh, H. Freedman, and G. Hanna, "A mixed quantum-classical liouville study of the population dynamics in a model photo-induced condensed phase electron transfer reaction," *The Journal of Chemical Physics*, vol. 138, no. 14, 2013.

[22] R. Crespo-Otero and M. Barbatti, "Recent advances and perspectives on nonadiabatic mixed quantum–classical dynamics," *Chemical reviews*, vol. 118, no. 15, pp. 7026–7068, 2018.

[23] J.-L. Liao and G. A. Voth, "A centroid molecular dynamics approach for nonadiabatic dynamical processes in condensed phases: The spin-boson case," *The Journal of Physical Chemistry B*, vol. 106, no. 33, pp. 8449–8455, 2002.

[24] H.-D. Meyer, U. Manthe, and L. Cederbaum, "The multi-configurational time-dependent Hartree approach," *Chemical Physics Letters*, vol. 165, no. 1, pp. 73–78, 1990.

[25] H. Wang, "Multilayer multiconfiguration time-dependent hartree theory," *The Journal of Physical Chemistry A*, vol. 119, no. 29, pp. 7951–7965, 2015.

[26] I. Burghardt, K. Giri, and G. Worth, "Multimode quantum dynamics using gaussian wavepackets: The gaussian-based multiconfiguration time-dependent hartree (g-mctdh) method applied to the absorption spectrum of pyrazine," *The Journal of Chemical Physics*, vol. 129, no. 17, 2008.

[27] M. Born and R. Oppenheimer, "On the quantum theory of molecules," in *Quantum Chemistry: Classic Scientific Papers*, pp. 1–24, World Scientific, 2000.

[28] G. D. Scholes, G. R. Fleming, A. Olaya-Castro, and R. Van Grondelle, "Lessons from nature about solar light harvesting," *Nature chemistry*, vol. 3, no. 10, pp. 763–774, 2011.

[29] X. Sun, P. Zhang, Y. Lai, K. L. Williams, M. S. Cheung, B. D. Dunietz, and E. Geva, "Computational study of charge-transfer dynamics in the carotenoid–porphyrin–c60 molecular triad solvated in explicit tetrahydrofuran and its spectroscopic signature," *The Journal of Physical Chemistry C*, vol. 122, no. 21, pp. 11288–11299, 2018.

[30] A. K. Manna, D. Balamurugan, M. S. Cheung, and B. D. Dunietz, "Unraveling the mechanism of photoinduced charge transfer in carotenoid–porphyrin–c60 molecular triad," *The Journal of Physical Chemistry Letters*, vol. 6, no. 7, pp. 1231–1237, 2015.

[31] C. Andrea Rozzi, S. Maria Falke, N. Spallanzani, A. Rubio, E. Molinari, D. Brida, M. Maiuri, G. Cerullo, H. Schramm, J. Christoffers, *et al.*, "Quantum coherence controls the charge separation in a prototypical artificial light-harvesting system," *Nature communications*, vol. 4, no. 1, p. 1602, 2013.

[32] H. Hashimoto, C. Uragami, and R. J. Cogdell, "Carotenoids and photosynthesis," *Carotenoids in nature: Biosynthesis, regulation and function*, pp. 111–139, 2016.

[33] B. S. Brunschwig and N. Sutin, "Energy surfaces, reorganization energies, and coupling elements in electron transfer," *Coordination chemistry reviews*, vol. 187, no. 1, pp. 233–254, 1999.

[34] H.-D. Meyer, F. Gatti, and G. A. Worth, *Multidimensional Quantum Dynamics: MCTDH Theory and Applications*. Weinheim: Wiley-VCH, 2009.

[35] F. Gatti, B. Lasorne, H.-D. Meyer, and A. Nauts, *Applications of Quantum Dynamics in Chemistry*, vol. 98 of *Lecture Notes in Chemistry*. Springer International Publishing, 2017.

[36] A. Raab, "On the dirac–frenkel/mclachlan variational principle," *Chemical physics letters*, vol. 319, no. 5-6, pp. 674–678, 2000.

[37] H.-D. Meyer and G. A. Worth, "Quantum molecular dynamics: propagating wavepackets and density operators using the multiconfiguration time-dependent hartree method," *Theoretical Chemistry Accounts*, vol. 109, pp. 251–267, 2003.

[38] H.-D. Meyer, "Introduction to mctdh," *Lecture Notes*, 2011.

[39] U. Manthe and F. Huarte-Larrañaga, "Partition functions for reaction rate calculations: statistical sampling and mctdh propagation," *Chemical physics letters*, vol. 349, no. 3-4, pp. 321–328, 2001.

[40] G. Worth, M. Beck, A. Jäckle, H. Meyer, F. Otto, M. Brill, and O. Vendrell, "The heidelberg mctdh package: A set of programs for multi-dimensional quantum dynamics," *User's Guide, Version*, vol. 8, 2000.

[41] E. Condon, "A theory of intensity distribution in band systems," *Physical Review*, vol. 28, no. 6, p. 1182, 1926.